

Development of the Kidney Model

For tissue fixation and dissection, the mouse was anesthetized with an overdose of ketamine-xylazine. Transcardial perfusion was performed with 0.1 M phosphate-buffered saline solution until the liver became brown and the fluid exiting the heart became clear, followed by a 4% PFA solution. Immediately after perfusion, the left kidney was excised from the mouse and was immersed in a 4% paraformaldehyde solution at 4 °C for one night for tissue preservation. Afterwards, the kidney was immersed for 48 hours in a 2.5 mM solution of Dotarem (gadolinium-based contrast agent; Guerbet) to enhance visibility of different renal tissues in the MR image. Lastly, the kidney was transferred to a phosphate-buffered saline with 0.1% of sodium azide for conservation and MR imaging.

MR imaging was performed at the Bio-Imaging Laboratory of the University of Antwerp (Belgium) with a horizontal 7-T preclinical scanner (PharmaScan; Bruker BioSpin) equipped with a homemade transmit receive linear volume resonator at 300 MHz using a T1-weighted rapid acquisition with relaxation enhancement (RARE) sequence (30-ms repetition time, 11-ms echo time, 100 excitations). The MR image resolution was 43x78x78 μm (anisotropic parallelepiped voxels).

Ten volume regions were segmented on the MR image using 3D Slicer software (<http://www.slicer.org>) both manually and with the aid of semi-automatic tools based on voxel intensity (e.g., threshold tool) and location (e.g., grow from seed tool) information. The segmented regions correspond to 4 tissues of the kidney parenchyma (namely the cortex, the outer stripe of the outer medulla (OSOM), the inner stripe of the outer medulla (ISOM) and the inner medulla (IM)), the major component of the vasculature within the kidney parenchyma, the papilla, the renal pelvis, part of the external renal vessels, part of the ureter and a uniform surrounding tissue. All segmented regions were merged into a single 3D matrix consisting of 127x62x125 (~ 1 million) voxels, with same voxel dimensions as the MR dataset.

Tissue segmentation was validated with conventional histology of the same kidney. To that end, after MR imaging, the kidney specimen was embedded in paraffin and sectioned (7- μm thickness) in the coronal plane. Sections were stained with hematoxylin and eosin (H&E) and were digitally imaged at 20x magnification using bright-field contrast on a Ti Eclipse inverted widefield microscope (Nikon Instruments Inc). Regions of interest (ROI) were drawn on the histological images over different kidney tissues and were visually compared against manually co-registered cross sections of the segmented 3D kidney model.

Calculation of S Values and Energy Absorbed Fractions

The 3D segmentation matrix was implemented in MCNP as a lattice of parallelepiped elements (voxels) using same lattice and voxel dimensions as the segmentation map. That lattice containing the kidney model was embedded inside a 24-mL region representing the mouse body, modelled as an elliptical cylinder capped by a half ellipsoid. All mouse regions (body and lattice with kidney) were modelled as 1.04-g.cm⁻³ soft tissue with elemental composition as in the adult human kidney model of MIRD Pamphlet 19 (3).

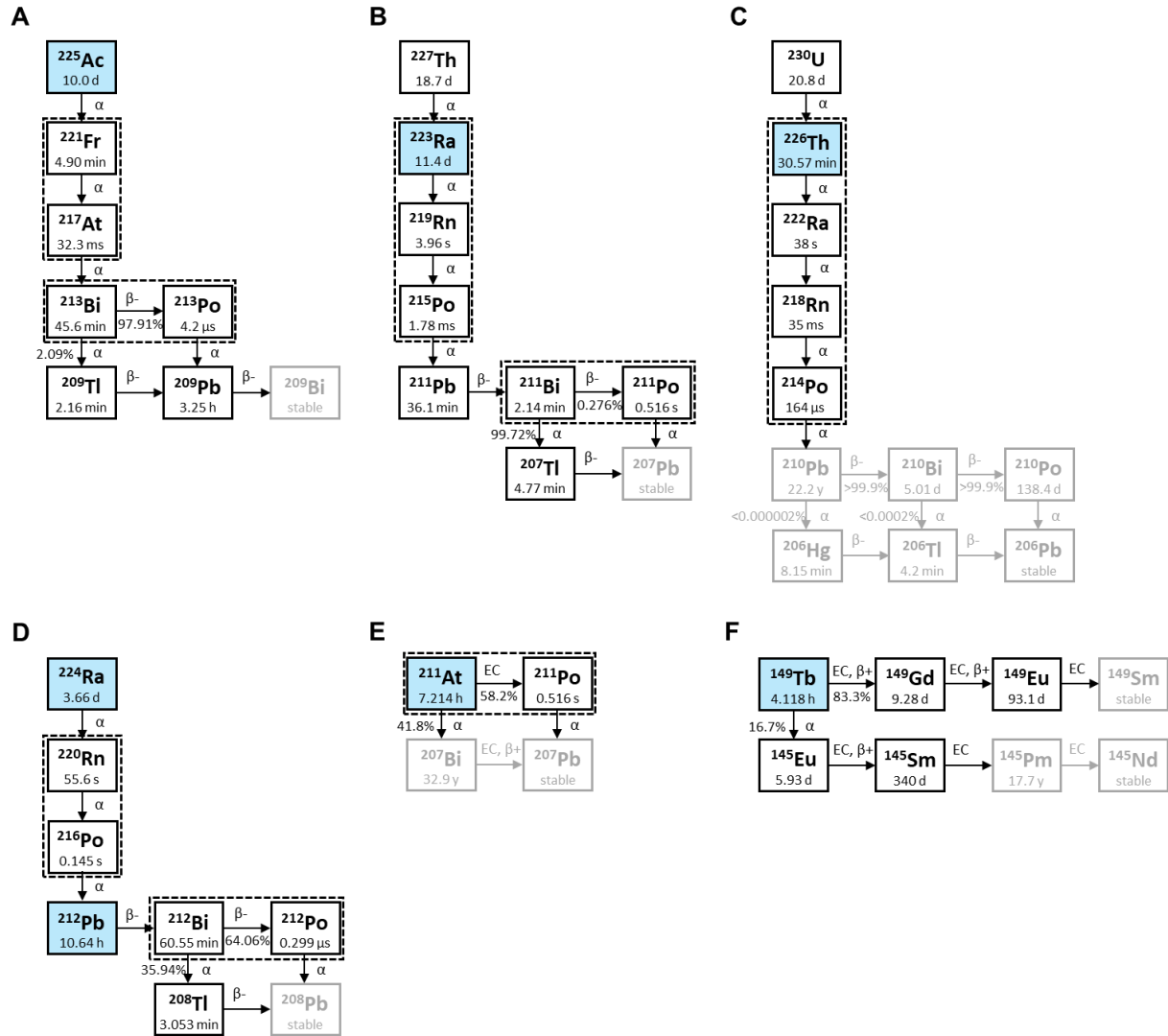
Radionuclide radiation emission data of ICRP Report 107 (10) was used for modelling the radiation sources. The simulated sources included photons (gamma- and X-rays), beta particles (beta- and positrons), Auger and internal conversion electrons and alpha particles. The kinetic energy of beta- particles and positrons emitted by the sources was sampled from a continuous spectrum based on linear interpolations of the energy–emission probability data of ICRP107.

MCNP cross-section libraries EPRDATA14 and ELO3 for photon and single-event electron/positron transport were used. Alpha-particle transport was based on the continuous slowing down approximation for energy loss. The cut-off energy (i.e., the limit at which the particle energy is regarded to be locally absorbed) was set to 1 keV for all particles.

Source regions (r_s) and target regions (r_T) for S value and absorbed fraction calculations include: the renal cortex including its vasculature (*C*), the outer stripe of the outer medulla including its vasculature (*OS*), the inner stripe of the outer medulla (*IS*), the inner medulla including some vasculature (*IM*) and the renal papilla and pelvis (*PP*). These regions, all together, represent the whole kidney region (*K*), which was used also as a source and target region in case of a uniform activity distribution throughout kidney tissues.

For each radionuclide, the activity was uniformly distributed in each of the source regions and the absorbed dose per decay was simulated using MCNP *F8 tally. For the radionuclide chains involving alpha emitters, only the descendants with a half-life shorter than 1 year were considered descendants (radionuclides shown in black color in Supplemental Figure S1). Therefore, S values were not calculated for ²⁰⁷Bi (descendant of ²¹¹At) and for ²¹⁰Pb (descendent of ²³⁰U) and its descendants. Also, the S-value contributions of short-lived (< 1 min) descendants of alpha emitters are included in the S values of the nearest parent isotope with a half-life longer than 1 min (radionuclides enclosed by a dashed line box in Supplemental Figure S1).

Monte Carlo simulations were performed in a parallel computer system (based on Intel Xeon Gold 6154 3.00 GHz processors running CentOS 7.8) using 72 threads. The number of source particles simulated for each radionuclide source region was at least 3.0E+06 for beta particles, 1.0E+07 for Auger and internal conversion electrons, 3.0E+07 for photons, and 1.0E+07 for alpha particles. As a reference, the computing times for 1.0E+06 simulated beta particles of ¹³¹I and ⁹⁰Y emitted from the cortex region were respectively 15 and 70 minutes.



SUPPLEMENTAL FIGURE 1. Decay schemes of various alpha emitters of interest in radiopharmaceutical therapy. The radionuclide decays enclosed by a dashed line box are considered as a single S value because of the short half-life (< 1 min) of the descendants.

Kidney Dosimetry Study

A dosimetry study was performed to demonstrate the use of the regional S values calculated with the kidney model. The radioligand used to derive the mouse kidney biodistribution was the iodinated anti-HER2 sdAb 2Rs15d, previously reported elsewhere (11).

All reagents were purchased from Sigma-Aldrich unless otherwise stated. Sodium [^{131}I]iodide was purchased from Perkin-Elmer. Anti-HER2 sdAb 2Rs15d was radiolabeled with ^{131}I via the residualizing prosthetic group N-Succinimidyl 4-guanodimethyl-3- ^{131}I iodobenzoate ([^{131}I]SGMIB) and purified as reported previously (11).

Healthy mice ($n=5$, C57BL/6, female, 9-week-old, 20.7 ± 1.0 g body-weight mean \pm standard deviation (SD)) were anesthetized by inhalation with 2% isoflurane and were intravenously injected in the tail vein with 13.0 ± 3.3 MBq ^{131}I -sdAb (5 μg sdAb). At 1, 3, 6, 24 and 70 h post injection (p.i.), mice ($n=1$ per time point) were euthanized by cervical dislocation. The kidneys were dissected, weighed and their activity was measured in a Cobra-II 5003 gamma counter (Canberra-Packard) using an optimized measurement protocol (12). Radioactivity in kidney was corrected for decay to the time of sacrifice. The fraction of injected activity per gram of dissected kidney tissue (FIA/g) was calculated.

The sub-organ distribution of ^{131}I -sdAb in kidney tissues was determined with high-resolution quantitative digital autoradiography using an iQID system (13). To that end, the kidney specimens were snap-frozen and cryostat-sectioned in 10- μm sections. For the autoradiography measurements, tissue sections were placed in contact with a scintillating screen based on terbium-doped gadolinium oxysulfide ($\text{Gd}_2\text{O}_2\text{S:Tb}$) phosphor (Kodak BioMax TranScreen LE; Carestream Health), which was used to convert the beta and electron emissions of ^{131}I into visible photons detectable by the iQID camera. Tissue sections were imaged for up to 10 hours. The resulting autoradiography images were corrected for decay to the time of sacrifice using ImageJ-Fiji software (<https://imagej.net/software/fiji/>). Each autoradiography image was quantified in ImageJ-Fiji using detailed ROIs drawn on histological images (H&E staining) of the same section used for autoradiography or an adjacent kidney section. A ROI was drawn on each of the 5 tissues considered as source regions in the kidney model (r_S : C, OS, IS, IM, PP) and the mean of the counts per minute (CPM) of the ROI pixels were estimated ($CPM(r_S)$).

Sub-organ regional dosimetry of kidney tissues was performed following the MIRD methodology. Two source distributions were considered: (i) a time-dependent heterogeneous activity distribution based on the relative autoradiography data, and (ii) the simplified case in which activity is assumed to be uniformly distributed throughout kidney tissues (*i.e.*, $r_S=r_T=K$). For each time point, the absorbed dose rate ($\dot{D}(r_T, t)$) in each target region r_T delivered by the activities in each source regions r_S of the kidney model was calculated, per unit of administered activity (A_0), as:

$$\dot{D}(r_T, t)/A_0 = \frac{1}{A_0} \cdot \frac{M_K}{\bar{M}_{kidney}} \cdot \sum_{r_S} A(r_S, t) \cdot S(r_T \leftarrow r_S) \quad (\text{Supplemental Eq. 1})$$

Where $A(r_S, t)$ is the activity in source region r_S at a time t p.i. of the radioligand; $S(r_T \leftarrow r_S)$ is the radionuclide-specific S value calculated for the proposed kidney model for the target/source regions r_T and r_S ; M_K is the mass of region K of the kidney model (0.1175 g, cf. Table 1); and \bar{M}_{kidney} is the average of the measured kidney masses of all ($n=5$) mice (0.1270 g). The kidney activities measured with gamma counting ($A(t)_{kidney}$) are affected by inter-mouse variability. To limit the effect of this in the dosimetry, normalized whole-

kidney activities ($A(t)_{\text{kidney_norm}}$) were calculated by multiplying the whole-kidney activities measured with gamma counting ($A(t)_{\text{kidney}}$) by a normalization factor $M(t)_{\text{kidney}}/\bar{M}_{\text{kidney}}$ (where $M(t)_{\text{kidney}}$ corresponds to the measured kidney mass corresponding to time point t). When the activity is uniformly distributed throughout kidney tissues ($r_s=K$), $A(r_s,t)$ is equal to the normalized whole-kidney activity $A(t)_{\text{kidney_norm}}$. To estimate $A(r_s,t)$ for the sub-kidney regions (Equation S2), the normalized kidney activity $A(t)_{\text{kidney_norm}}$ was allocated to the different source regions of the kidney model according to the relative $CPM(r_s)$ values determined with autoradiography and the percentage volume occupancy of region r_s in region K of the kidney model ($\%V(r_s)$) (cf. Table 1).

$$A(r_s, t) = \%V(r_s) \cdot A(t)_{\text{kidney_norm}} \cdot \frac{CPM_{r_s}}{\sum_{r_s} CPM(r_s) \cdot \%V(r_s)} \quad (\text{Supplemental Eq. 2})$$

Thus, the relative activity concentrations of the different compartments of the kidney model are assumed to be the same as the relative intensity densities of the different tissue ROIs of the autoradiography images.

Values of $\dot{D}(r_T, t)/A_0$ as a function of time elapsed p.i. (t) were analyzed by nonlinear least squares fitting (MATLAB, MathWorks). The Pearson's correlation coefficient (R^2) was used to quantify goodness of fit. Initially, various mathematical functions were considered for analyzing the time dependence of $\dot{D}(r_T, t)/A_0$, including negative exponentials with or without a positive baseline (mathematical form: $f(t) = a \cdot e^{(-b \cdot t)}$; $f(t) = a \cdot e^{(-b \cdot t)} + d$), a sum of two negative exponentials ($f(t) = a \cdot e^{(-b \cdot t)} + g \cdot e^{(-h \cdot t)}$), and a single negative power function with and without a positive baseline ($f(t) = c_1 \cdot t^{-c_2}$; $f(t) = c_3 \cdot t^{-c_4} + c_5$). A previous investigation (not reported in this work) evaluated the sensitivity of each function model to a few subsets of data points selected from a larger dataset of $\dot{D}(K, t)/A_0$ of the kidney for an assumed uniform activity in kidney tissues (e.g., data subsets considering variations in the number of time points or in the number of mice per time point). In that investigation, from the functions considered, the negative power function resulted in the lowest variability in the estimation of the time-integrated absorbed dose per unit of injected activity from the different subsets of dose rate data, and showed an R^2 very similar to that of other (more complex) function models (e.g. difference in R^2 of less than 0.004 compared to a bi-exponential model, for the subsets of data considered). The R^2 of the $\dot{D}(r_T, t)/A_0$ data of specific kidney tissues for the heterogeneous activity distribution showed similar results (difference in R^2 of less than 0.001 between bi-exponential and power fits). Therefore, in this study a negative power function of time t with two coefficients (c_1 and c_2) (Equation S3) was chosen to model the time dependence of all the $\dot{D}(r_T, t)/A_0$ datasets.

$$\dot{D}(r_T, t)/A_0 \cong c_1 t^{-c_2} \quad (\text{Supplemental Eq. 3})$$

For each of the two source distributions considered, the mean absorbed dose ($D(r_T)$) per unit of administered activity ($D(r_T)/A_0$) was estimated for each target region applying mathematical integration of dose rate values from the time of injection ($t=0$) to infinity in two parts. Absorbed dose rates were assumed to be zero at $t=0$ and to increase linearly over time until a peak value at $t=1$ h (earliest time point measured), which was calculated from the power function fit. From $t=1$ h until infinity, kidney uptake was assumed to follow the power function fit. (The dose contribution of the period of time from the last measured time point (70 h) until infinity was verified to be lower than the dose contribution resulting from assuming only physical ^{131}I decay from 70 h p.i. on).

Segmentation of the Kidney Model Regions

There is a good agreement between the histology-based tissue ROIs and the MR-based ROIs used to define the kidney model (Figure 3 A). The sharp contrast in the MR data of the IM and ISOM, the ISOM and OSOM, and the largest blood vessels and kidney parenchyma facilitated the delineation of the boundary between these tissues. However, because of the poor contrast in the MR data of cortical and OSOM tissues, the cortex–OSOM boundary in the kidney model is smoother than the microscopically detailed boundary defined in histological images based on the presence of glomeruli (zoom-in subfigure in Figure 3 A). Yet the dimensions and overall extension of the OSOM tissue are well represented in the kidney model. The level of detail with which the internal vasculature could be segmented is limited by the spatial resolution of MR data. Because of this, only part of the vasculature tree is represented in the kidney model, where the thickest vessels (cf. Figure 3 B) correspond to pairs of arteries and veins located close to each other.

SUPPLEMENTAL TABLE 1. S values of beta- emitters.

$r_T \leftarrow r_S$	S values ($mGy.MBq^{-1}.s^{-1}$)											
	¹⁷⁷ Lu	⁶⁷ Cu	¹⁶¹ Tb	⁴⁷ Sc	¹³¹ I	¹⁵³ Sm	¹⁸⁶ Re	⁸⁹ Sr	¹⁶⁶ Ho	³² P	¹⁸⁸ Re	⁹⁰ Y
<i>K</i> ← <i>K</i>	1.89E-01	1.93E-01	2.61E-01	2.03E-01	2.38E-01	3.28E-01	3.84E-01	4.85E-01	5.45E-01	5.34E-01	5.51E-01	5.56E-01
<i>C</i> ← <i>C</i>	3.10E-01	3.20E-01	4.36E-01	3.20E-01	3.56E-01	4.94E-01	4.81E-01	5.15E-01	6.06E-01	5.47E-01	5.83E-01	5.62E-01
<i>OS</i> ← <i>C</i>	5.28E-02	5.24E-02	6.68E-02	6.94E-02	9.53E-02	1.26E-01	2.17E-01	3.36E-01	3.58E-01	3.84E-01	3.87E-01	4.14E-01
<i>IS</i> ← <i>C</i>	2.38E-03	2.83E-03	4.26E-03	5.07E-03	1.23E-02	2.35E-02	9.53E-02	2.37E-01	2.63E-01	2.87E-01	2.95E-01	3.32E-01
<i>IM</i> ← <i>C</i>	2.25E-03	2.66E-03	3.78E-03	4.34E-03	9.94E-03	1.74E-02	7.28E-02	2.06E-01	2.36E-01	2.55E-01	2.69E-01	3.10E-01
<i>PP</i> ← <i>C</i>	1.94E-02	1.95E-02	2.52E-02	2.65E-02	3.91E-02	5.40E-02	1.14E-01	2.24E-01	2.53E-01	2.70E-01	2.83E-01	3.19E-01
<i>K</i> ← <i>C</i>	1.76E-01	1.81E-01	2.46E-01	1.87E-01	2.15E-01	2.97E-01	3.31E-01	4.10E-01	4.69E-01	4.50E-01	4.71E-01	4.76E-01
<i>C</i> ← <i>OS</i>	5.28E-02	5.24E-02	6.68E-02	6.94E-02	9.53E-02	1.26E-01	2.17E-01	3.36E-01	3.58E-01	3.84E-01	3.87E-01	4.14E-01
<i>OS</i> ← <i>OS</i>	5.00E-01	5.15E-01	7.04E-01	5.17E-01	5.75E-01	7.99E-01	7.86E-01	8.41E-01	9.80E-01	8.89E-01	9.37E-01	8.91E-01
<i>IS</i> ← <i>OS</i>	9.86E-02	9.80E-02	1.24E-01	1.29E-01	1.78E-01	2.40E-01	4.22E-01	6.23E-01	6.49E-01	7.00E-01	6.88E-01	7.15E-01
<i>IM</i> ← <i>OS</i>	4.27E-02	4.15E-02	5.78E-02	6.16E-02	9.59E-02	1.37E-01	2.99E-01	5.20E-01	5.51E-01	6.03E-01	5.95E-01	6.35E-01
<i>PP</i> ← <i>OS</i>	7.48E-02	7.54E-02	9.29E-02	9.56E-02	1.27E-01	1.66E-01	2.89E-01	4.64E-01	4.96E-01	5.32E-01	5.36E-01	5.69E-01
<i>K</i> ← <i>OS</i>	2.02E-01	2.06E-01	2.78E-01	2.20E-01	2.60E-01	3.56E-01	4.29E-01	5.41E-01	6.02E-01	5.94E-01	6.09E-01	6.14E-01
<i>C</i> ← <i>IS</i>	2.38E-03	2.83E-03	4.26E-03	5.07E-03	1.23E-02	2.35E-02	9.53E-02	2.37E-01	2.63E-01	2.87E-01	2.95E-01	3.32E-01
<i>OS</i> ← <i>IS</i>	9.86E-02	9.80E-02	1.24E-01	1.29E-01	1.78E-01	2.40E-01	4.22E-01	6.23E-01	6.49E-01	7.00E-01	6.88E-01	7.15E-01
<i>IS</i> ← <i>IS</i>	1.19E+00	1.22E+00	1.67E+00	1.25E+00	1.40E+00	1.94E+00	1.92E+00	1.93E+00	2.21E+00	2.00E+00	2.09E+00	1.93E+00
<i>IM</i> ← <i>IS</i>	1.91E-01	1.89E-01	2.42E-01	2.52E-01	3.47E-01	4.63E-01	7.87E-01	1.09E+00	1.12E+00	1.21E+00	1.17E+00	1.20E+00
<i>PP</i> ← <i>IS</i>	4.72E-02	4.82E-02	5.96E-02	6.18E-02	8.76E-02	1.26E-01	2.86E-01	5.32E-01	5.67E-01	6.19E-01	6.16E-01	6.58E-01
<i>K</i> ← <i>IS</i>	2.03E-01	2.07E-01	2.80E-01	2.23E-01	2.66E-01	3.68E-01	4.68E-01	6.15E-01	6.77E-01	6.79E-01	6.90E-01	6.97E-01
<i>C</i> ← <i>IM</i>	2.25E-03	2.66E-03	3.78E-03	4.34E-03	9.94E-03	1.74E-02	7.28E-02	2.06E-01	2.36E-01	2.55E-01	2.69E-01	3.10E-01
<i>OS</i> ← <i>IM</i>	4.27E-02	4.15E-02	5.78E-02	6.16E-02	9.59E-02	1.37E-01	2.99E-01	5.20E-01	5.51E-01	6.03E-01	5.95E-01	6.35E-01
<i>IS</i> ← <i>IM</i>	1.91E-01	1.89E-01	2.42E-01	2.52E-01	3.47E-01	4.63E-01	7.87E-01	1.09E+00	1.12E+00	1.21E+00	1.17E+00	1.20E+00
<i>IM</i> ← <i>IM</i>	8.37E+00	8.64E+00	1.19E+01	8.41E+00	9.05E+00	1.27E+01	1.07E+01	9.16E+00	1.13E+01	9.11E+00	9.95E+00	8.58E+00
<i>PP</i> ← <i>IM</i>	1.41E+00	1.43E+00	1.68E+00	1.70E+00	2.05E+00	2.52E+00	3.25E+00	3.53E+00	3.60E+00	3.71E+00	3.66E+00	3.51E+00
<i>K</i> ← <i>IM</i>	2.03E-01	2.07E-01	2.80E-01	2.23E-01	2.66E-01	3.67E-01	4.67E-01	6.26E-01	6.92E-01	6.95E-01	7.08E-01	7.20E-01
<i>C</i> ← <i>PP</i>	1.94E-02	1.95E-02	2.52E-02	2.65E-02	3.91E-02	5.40E-02	1.14E-01	2.24E-01	2.53E-01	2.70E-01	2.83E-01	3.19E-01
<i>OS</i> ← <i>PP</i>	7.48E-02	7.54E-02	9.29E-02	9.56E-02	1.27E-01	1.66E-01	2.89E-01	4.64E-01	4.96E-01	5.32E-01	5.36E-01	5.69E-01
<i>IS</i> ← <i>PP</i>	4.72E-02	4.82E-02	5.96E-02	6.18E-02	8.76E-02	1.26E-01	2.86E-01	5.32E-01	5.67E-01	6.19E-01	6.16E-01	6.58E-01
<i>IM</i> ← <i>PP</i>	1.41E+00	1.43E+00	1.68E+00	1.70E+00	2.05E+00	2.52E+00	3.25E+00	3.53E+00	3.60E+00	3.71E+00	3.66E+00	3.51E+00
<i>PP</i> ← <i>PP</i>	9.80E+00	1.01E+01	1.44E+01	9.65E+00	1.04E+01	1.50E+01	1.21E+01	1.03E+01	1.30E+01	1.02E+01	1.12E+01	9.56E+00
<i>K</i> ← <i>PP</i>	1.89E-01	1.93E-01	2.62E-01	2.04E-01	2.40E-01	3.32E-01	4.00E-01	5.29E-01	5.94E-01	5.87E-01	6.06E-01	6.18E-01

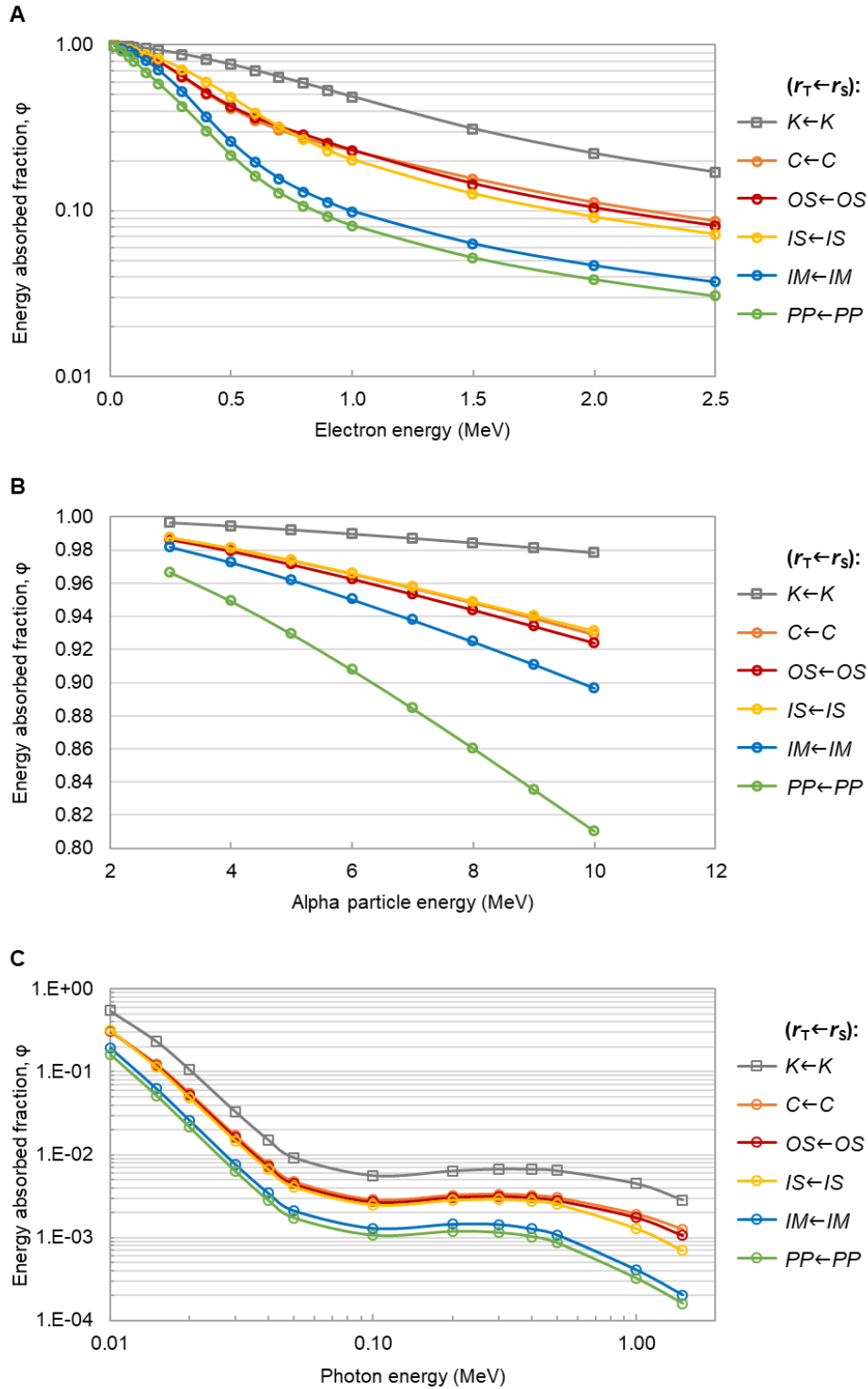
SUPPLEMENTAL TABLE 2. S values of some alpha emitters and their decay progenies.

$r_T \leftarrow r_S$	S values ($mGy.MBq^{-1}.s^{-1}$)										
	^{225}Ac	^{221}Fr (incl. ^{217}At)	^{213}Bi (incl. ^{213}Po)	^{209}Tl	^{209}Pb	^{227}Th	^{223}Ra (incl. $^{219}Rn, ^{215}Po$)	^{211}Pb	^{211}Bi (incl. ^{211}Po)	^{207}Tl	^{211}At (incl. ^{211}Po)
$K \leftarrow K$	7.85E+00	1.80E+01	1.16E+01	5.51E-01	2.38E-01	8.05E+00	2.68E+01	4.24E-01	9.08E+00	4.47E-01	9.15E+00
$C \leftarrow C$	1.50E+01	3.42E+01	2.14E+01	5.94E-01	3.51E-01	1.53E+01	5.08E+01	4.80E-01	1.72E+01	4.92E-01	1.73E+01
$OS \leftarrow C$	3.35E-01	9.55E-01	1.08E+00	3.78E-01	1.00E-01	3.60E-01	1.42E+00	2.73E-01	5.39E-01	2.96E-01	5.02E-01
$IS \leftarrow C$	6.91E-04	2.41E-04	1.52E-01	2.72E-01	1.31E-02	2.42E-03	2.19E-03	1.64E-01	7.11E-03	1.88E-01	8.54E-04
$IM \leftarrow C$	6.40E-04	2.48E-04	1.26E-01	2.43E-01	9.87E-03	2.33E-03	2.16E-03	1.36E-01	5.84E-03	1.57E-01	7.83E-04
$PP \leftarrow C$	1.10E-01	3.15E-01	4.32E-01	2.63E-01	4.08E-02	1.19E-01	4.71E-01	1.66E-01	1.82E-01	1.86E-01	1.66E-01
$K \leftarrow C$	7.78E+00	1.78E+01	1.14E+01	4.70E-01	2.14E-01	7.97E+00	2.65E+01	3.60E-01	8.96E+00	3.78E-01	9.04E+00
$C \leftarrow OS$	3.35E-01	9.55E-01	1.08E+00	3.78E-01	1.00E-01	3.60E-01	1.42E+00	2.73E-01	5.39E-01	2.96E-01	5.02E-01
$OS \leftarrow OS$	2.41E+01	5.49E+01	3.44E+01	9.61E-01	5.68E-01	2.46E+01	8.16E+01	7.86E-01	2.75E+01	8.06E-01	2.78E+01
$IS \leftarrow OS$	7.25E-01	2.07E+00	2.27E+00	6.85E-01	1.89E-01	7.75E-01	3.08E+00	5.19E-01	1.14E+00	5.62E-01	1.09E+00
$IM \leftarrow OS$	4.77E-02	1.36E-01	5.20E-01	5.80E-01	1.03E-01	5.85E-02	2.13E-01	4.08E-01	1.44E-01	4.52E-01	7.26E-02
$PP \leftarrow OS$	6.46E-01	1.85E+00	1.94E+00	5.21E-01	1.33E-01	6.89E-01	2.75E+00	3.71E-01	9.93E-01	4.06E-01	9.72E-01
$K \leftarrow OS$	7.93E+00	1.83E+01	1.18E+01	6.11E-01	2.62E-01	8.13E+00	2.71E+01	4.74E-01	9.21E+00	5.00E-01	9.26E+00
$C \leftarrow IS$	6.91E-04	2.41E-04	1.52E-01	2.72E-01	1.31E-02	2.42E-03	2.19E-03	1.64E-01	7.11E-03	1.88E-01	8.54E-04
$OS \leftarrow IS$	7.25E-01	2.07E+00	2.27E+00	6.85E-01	1.89E-01	7.75E-01	3.08E+00	5.19E-01	1.14E+00	5.62E-01	1.09E+00
$IS \leftarrow IS$	5.49E+01	1.25E+02	7.88E+01	2.18E+00	1.39E+00	5.62E+01	1.86E+02	1.86E+00	6.29E+01	1.90E+00	6.35E+01
$IM \leftarrow IS$	1.11E+00	3.18E+00	3.65E+00	1.19E+00	3.70E-01	1.20E+00	4.75E+00	9.35E-01	1.82E+00	1.00E+00	1.67E+00
$PP \leftarrow IS$	4.56E-01	1.31E+00	1.52E+00	5.92E-01	9.27E-02	4.87E-01	1.95E+00	4.09E-01	6.98E-01	4.53E-01	6.92E-01
$K \leftarrow IS$	7.93E+00	1.83E+01	1.19E+01	6.91E-01	2.69E-01	8.13E+00	2.71E+01	5.31E-01	9.21E+00	5.64E-01	9.26E+00
$C \leftarrow IM$	6.40E-04	2.48E-04	1.26E-01	2.43E-01	9.87E-03	2.33E-03	2.16E-03	1.36E-01	5.84E-03	1.57E-01	7.83E-04
$OS \leftarrow IM$	4.77E-02	1.36E-01	5.20E-01	5.80E-01	1.03E-01	5.85E-02	2.13E-01	4.08E-01	1.44E-01	4.52E-01	7.26E-02
$IS \leftarrow IM$	1.11E+00	3.18E+00	3.65E+00	1.19E+00	3.70E-01	1.20E+00	4.75E+00	9.35E-01	1.82E+00	1.00E+00	1.67E+00
$IM \leftarrow IM$	4.40E+02	1.00E+03	6.19E+02	1.06E+01	8.84E+00	4.51E+02	1.49E+03	9.46E+00	5.02E+02	9.37E+00	5.07E+02
$PP \leftarrow IM$	1.60E+01	4.59E+01	4.24E+01	3.80E+00	2.12E+00	1.70E+01	6.82E+01	3.35E+00	2.38E+01	3.47E+00	2.41E+01
$K \leftarrow IM$	7.93E+00	1.83E+01	1.19E+01	7.06E-01	2.68E-01	8.13E+00	2.71E+01	5.35E-01	9.21E+00	5.69E-01	9.26E+00
$C \leftarrow PP$	1.10E-01	3.15E-01	4.32E-01	2.63E-01	4.08E-02	1.19E-01	4.71E-01	1.66E-01	1.82E-01	1.86E-01	1.66E-01
$OS \leftarrow PP$	6.46E-01	1.85E+00	1.94E+00	5.21E-01	1.33E-01	6.89E-01	2.75E+00	3.71E-01	9.93E-01	4.06E-01	9.72E-01
$IS \leftarrow PP$	4.56E-01	1.31E+00	1.52E+00	5.92E-01	9.27E-02	4.87E-01	1.95E+00	4.09E-01	6.98E-01	4.53E-01	6.92E-01
$IM \leftarrow PP$	1.60E+01	4.59E+01	4.24E+01	3.80E+00	2.12E+00	1.70E+01	6.82E+01	3.35E+00	2.38E+01	3.47E+00	2.41E+01
$PP \leftarrow PP$	5.71E+02	1.28E+03	7.74E+02	1.20E+01	1.01E+01	5.83E+02	1.91E+03	1.06E+01	6.42E+02	1.05E+01	6.48E+02
$K \leftarrow PP$	7.84E+00	1.80E+01	1.16E+01	6.02E-01	2.40E-01	8.04E+00	2.67E+01	4.53E-01	9.06E+00	4.81E-01	9.13E+00

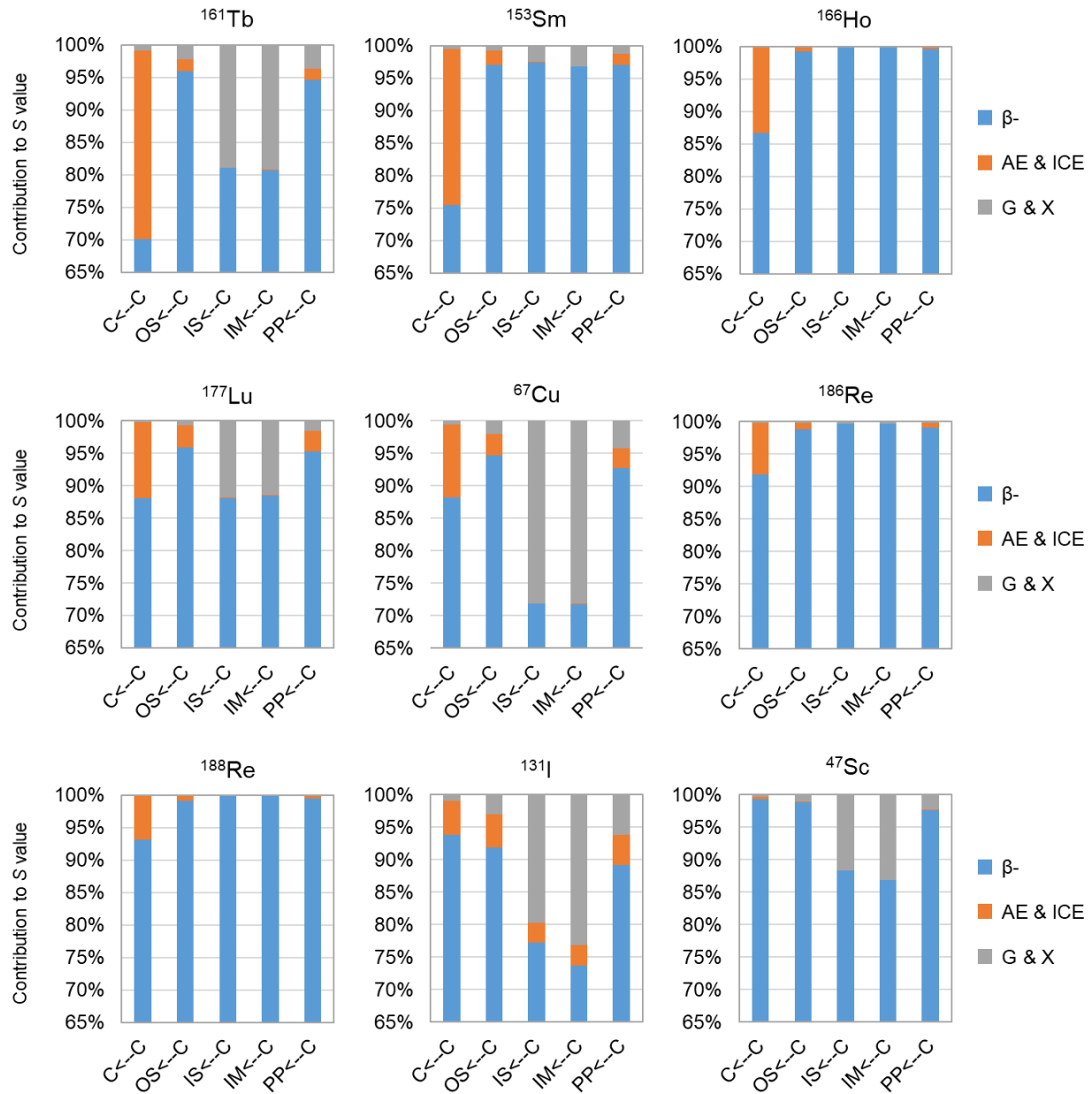
SUPPLEMENTAL TABLE 3. S values of some alpha emitters and their decay progenies.

$r_T \leftarrow r_S$	S values ($mGy.MBq^{-1}.s^{-1}$)											
	^{224}Ra	^{220}Rn (incl. ^{216}Po)	^{212}Pb	^{212}Bi (incl. ^{212}Po)	^{208}Tl	^{149}Tb	^{149}Gd	^{149}Eu	^{145}Eu	^{145}Sm	^{230}U	^{226}Th (incl. ^{222}Ra , ^{218}Rn , ^{214}Po)
$K \leftarrow K$	7.67E+00	1.76E+01	1.33E-01	1.10E+01	5.19E-01	9.92E-01	9.43E-02	3.55E-02	3.48E-02	4.50E-02	7.95E+00	3.73E+01
$C \leftarrow C$	1.46E+01	3.34E+01	2.28E-01	2.02E+01	5.66E-01	1.86E+00	1.57E-01	6.64E-02	4.79E-02	8.54E-02	1.52E+01	7.06E+01
$OS \leftarrow C$	3.18E-01	8.96E-01	2.92E-02	1.09E+00	3.51E-01	6.84E-02	2.46E-02	2.52E-03	1.60E-02	2.16E-03	3.46E-01	2.08E+00
$IS \leftarrow C$	7.51E-05	7.80E-06	1.48E-03	2.85E-01	2.33E-01	2.99E-02	4.49E-03	8.01E-04	1.25E-02	9.19E-04	3.35E-04	3.36E-04
$IM \leftarrow C$	7.82E-05	7.20E-06*	1.40E-03	2.62E-01	2.02E-01	2.67E-02	4.31E-03	7.45E-04	1.14E-02	8.64E-04	3.14E-04	3.32E-04
$PP \leftarrow C$	1.03E-01	2.95E-01	1.09E-02	5.16E-01	2.31E-01	3.79E-02	1.09E-02	1.31E-03	1.20E-02	1.24E-03	1.13E-01	6.89E-01
$K \leftarrow C$	7.60E+00	1.74E+01	1.26E-01	1.08E+01	4.41E-01	9.78E-01	8.90E-02	3.50E-02	3.17E-02	4.46E-02	7.87E+00	3.68E+01
$C \leftarrow OS$	3.18E-01	8.96E-01	2.92E-02	1.09E+00	3.51E-01	6.84E-02	2.46E-02	2.52E-03	1.60E-02	2.16E-03	3.46E-01	2.08E+00
$OS \leftarrow OS$	2.35E+01	5.37E+01	3.66E-01	3.24E+01	9.20E-01	2.98E+00	2.52E-01	1.07E-01	7.63E-02	1.37E-01	2.43E+01	1.13E+02
$IS \leftarrow OS$	6.87E-01	1.94E+00	5.53E-02	2.21E+00	6.50E-01	1.32E-01	4.52E-02	4.51E-03	2.76E-02	3.96E-03	7.48E-01	4.51E+00
$IM \leftarrow OS$	4.45E-02	1.25E-01	2.04E-02	6.77E-01	5.30E-01	6.86E-02	2.23E-02	2.65E-03	2.37E-02	2.11E-03	4.84E-02	2.95E-01
$PP \leftarrow OS$	6.12E-01	1.73E+00	4.42E-02	1.91E+00	4.79E-01	1.07E-01	3.49E-02	3.47E-03	2.19E-02	3.25E-03	6.67E-01	4.03E+00
$K \leftarrow OS$	7.74E+00	1.78E+01	1.40E-01	1.12E+01	5.79E-01	1.00E+00	9.99E-02	3.60E-02	3.70E-02	4.54E-02	8.03E+00	3.78E+01
$C \leftarrow IS$	7.51E-05	7.80E-06	1.48E-03	2.85E-01	2.33E-01	2.99E-02	4.49E-03	8.01E-04	1.25E-02	9.19E-04	3.35E-04	3.36E-04
$OS \leftarrow IS$	6.87E-01	1.94E+00	5.53E-02	2.21E+00	6.50E-01	1.32E-01	4.52E-02	4.51E-03	2.76E-02	3.96E-03	7.48E-01	4.51E+00
$IS \leftarrow IS$	5.36E+01	1.23E+02	8.60E-01	7.41E+01	2.14E+00	6.80E+00	5.91E-01	2.44E-01	1.70E-01	3.13E-01	5.55E+01	2.59E+02
$IM \leftarrow IS$	1.06E+00	2.99E+00	1.05E-01	3.53E+00	1.15E+00	2.19E-01	8.40E-02	8.28E-03	4.57E-02	6.63E-03	1.15E+00	6.94E+00
$PP \leftarrow IS$	4.31E-01	1.23E+00	2.86E-02	1.59E+00	5.35E-01	9.85E-02	2.52E-02	2.76E-03	2.48E-02	2.84E-03	4.70E-01	2.87E+00
$K \leftarrow IS$	7.74E+00	1.78E+01	1.41E-01	1.13E+01	6.52E-01	1.01E+00	1.01E-01	3.62E-02	4.01E-02	4.56E-02	8.03E+00	3.78E+01
$C \leftarrow IM$	7.82E-05	7.20E-06*	1.40E-03	2.62E-01	2.02E-01	2.67E-02	4.31E-03	7.45E-04	1.14E-02	8.64E-04	3.14E-04	3.32E-04
$OS \leftarrow IM$	4.45E-02	1.25E-01	2.04E-02	6.77E-01	5.30E-01	6.86E-02	2.23E-02	2.65E-03	2.37E-02	2.11E-03	4.84E-02	2.95E-01
$IS \leftarrow IM$	1.06E+00	2.99E+00	1.05E-01	3.53E+00	1.15E+00	2.19E-01	8.40E-02	8.28E-03	4.57E-02	6.63E-03	1.15E+00	6.94E+00
$IM \leftarrow IM$	4.31E+02	9.80E+02	6.28E+00	5.82E+02	1.04E+01	5.41E+01	4.25E+00	1.94E+00	1.11E+00	2.51E+00	4.45E+02	2.07E+03
$PP \leftarrow IM$	1.52E+01	4.31E+01	8.84E-01	3.80E+01	3.88E+00	1.63E+00	5.87E-01	4.95E-02	1.49E-01	4.82E-02	1.66E+01	1.00E+02
$K \leftarrow IM$	7.74E+00	1.78E+01	1.41E-01	1.13E+01	6.61E-01	1.01E+00	1.01E-01	3.62E-02	4.08E-02	4.57E-02	8.03E+00	3.78E+01
$C \leftarrow PP$	1.03E-01	2.95E-01	1.09E-02	5.16E-01	2.31E-01	3.79E-02	1.09E-02	1.31E-03	1.20E-02	1.24E-03	1.13E-01	6.89E-01
$OS \leftarrow PP$	6.12E-01	1.73E+00	4.42E-02	1.91E+00	4.79E-01	1.07E-01	3.49E-02	3.47E-03	2.19E-02	3.25E-03	6.67E-01	4.03E+00
$IS \leftarrow PP$	4.31E-01	1.23E+00	2.86E-02	1.59E+00	5.35E-01	9.85E-02	2.52E-02	2.76E-03	2.48E-02	2.84E-03	4.70E-01	2.87E+00
$IM \leftarrow PP$	1.52E+01	4.31E+01	8.84E-01	3.80E+01	3.88E+00	1.63E+00	5.87E-01	4.95E-02	1.49E-01	4.82E-02	1.66E+01	1.00E+02
$PP \leftarrow PP$	5.59E+02	1.26E+03	7.42E+00	7.31E+02	1.17E+01	7.11E+01	5.11E+00	2.57E+00	1.40E+00	3.33E+00	5.77E+02	2.64E+03
$K \leftarrow PP$	7.65E+00	1.76E+01	1.33E-01	1.10E+01	5.61E-01	9.96E-01	9.50E-02	3.56E-02	3.69E-02	4.51E-02	7.93E+00	3.72E+01

* Simulation error within 10%.



SUPPLEMENTAL FIGURE 2. Energy absorbed fractions (ϕ) for monoenergetic electrons (A), monoenergetic alpha particles (B) and monoenergetic photons (C), for self-irradiation. Data points are connected by smooth lines.



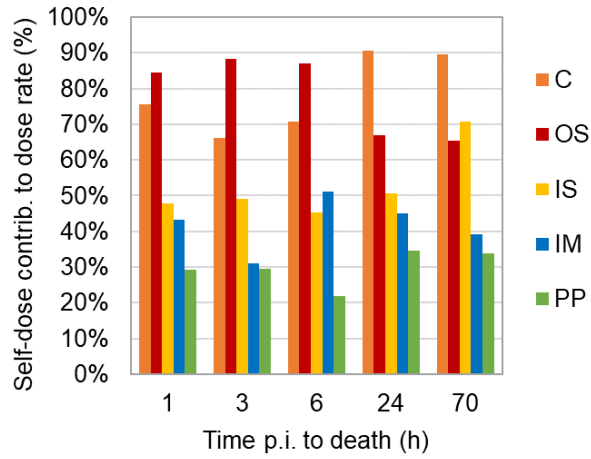
SUPPLEMENTAL FIGURE 3. Contribution of different radiation types (AE & IEC: Auger and internal conversion electrons; β^- : beta- particles; G & X: gamma- and X-rays) to the S values of some beta emitters.

SUPPLEMENTAL TABLE 4. Fraction of injected activity per gram (FIA/g) of dissected kidney and percentage of the normalized whole kidney activity ($A_{\text{kidney_norm}}$) allocated to each source tissue region, for the different time points of the ^{131}I -sdAb pharmacokinetics.

Time point (h)	FIA/g (g^{-1})	$A(r_s)/A_{\text{kidney_norm}} * 100$ (%)				
		<i>C</i>	<i>OS</i>	<i>IS</i>	<i>IM</i>	<i>PP</i>
1	4.36E-01	43%	50%	6%	<1%	<1%
3	5.32E-02	32%	60%	8%	<1%	<1%
6	1.82E-02	37%	56%	6%	1%	<1%
24	1.48E-03	69%	26%	4%	<1%	<1%
70	4.92E-04	63%	26%	10%	<1%	<1%

SUPPLEMENTAL TABLE 5. Coefficients of the power functions used to fit the time–absorbed dose rate per injected activity data of each target tissue region, for the two source distributions considered. R^2 values were always > 0.999.

r_s	r_T	Function coefficients	
		c_1 ($mGy.h^{-1}.MBq^{-1}$)	c_2
<i>K</i> (unif)	<i>K</i>	43.8	1.89
non-unif	<i>K</i>	44.4	1.87
non-unif	<i>C</i>	36.9	2.02
non-unif	<i>OS</i>	62.8	1.78
non-unif	<i>IS</i>	34.2	1.76
non-unif	<i>IM</i>	26.7	1.90
non-unif	<i>PP</i>	26.1	1.85



SUPPLEMENTAL FIGURE 4. Contribution of self-irradiation to the time-dependent absorbed dose rate of different kidney tissue regions (*C, OS, IS, IM, PP*).